Cellular/Molecular

CIB2 and CIB3 Regulate Stereocilia Maintenance and Mechanoelectrical Transduction in Mouse Vestibular Hair Cells

Xiaoying Wang,[1*] Shuang Liu,[2,3*] Qi Cheng,[1] Chengli Qu,[1] Rui Ren,[1] Haibo Du,[1] Nana Li,[1] Keji Yan,[1] Yanfei Wang,[1] Wei Xiong,[2,3] and Zhigang Xu[1,4]

[1]Shandong Provincial Key Laboratory of Animal Cells and Developmental Biology and Key Laboratory for Experimental Teratology of the Ministry of Education, School of Life Sciences, Shandong University, Qingdao, Shandong 266237, People's Republic of China, [2]School of Life Sciences, IDG/McGovern Institute for Brain Research, Tsinghua University, Beijing 100084, People's Republic of China, [3]Chinese Institute for Brain Research, Beijing 102206, People's Republic of China, and [4]Shandong Provincial Collaborative Innovation Center of Cell Biology, Shandong Normal University, Jinan, Shandong 250014, People's Republic of China

The mechanoelectrical transduction (MET) protein complex in the inner-ear hair cells is essential for hearing and balance perception. Calcium and integrin-binding protein 2 (CIB2) has been reported to be a component of MET complex, and loss of CIB2 completely abolishes MET currents in auditory hair cells, causing profound congenital hearing loss. However, loss of CIB2 does not affect MET currents in vestibular hair cells (VHCs) as well as general balance function. Here, we show that CIB2 and CIB3 act redundantly to regulate MET in VHCs, as MET currents are completely abolished in the VHCs of *Cib2*/*Cib3* double knock-out mice of either sex. Furthermore, we show that *Cib2* and *Cib3* transcripts have complementary expression patterns in the vestibular maculae, and that they play different roles in stereocilia maintenance in VHCs. *Cib2* transcripts are highly expressed in the striolar region, and knock-out of *Cib2* affects stereocilia maintenance in striolar VHCs. In contrast, *Cib3* transcripts are highly expressed in the extrastriolar region, and knock-out of *Cib3* mainly affects stereocilia maintenance in extrastriolar VHCs. Simultaneous knock-out of *Cib2* and *Cib3* affects stereocilia maintenance in all VHCs and leads to severe balance deficits. Taken together, our present work reveals that CIB2 and CIB3 are important for stereocilia maintenance as well as MET in mouse VHCs.

Key words: **CIB2; CIB3; mechanoelectrical transduction; stereocilia; vestibular hair cells**

Significance Statement

Calcium and integrin-binding protein 2 (CIB2) is an important component of mechanoelectrical transduction (MET) complex, and loss of CIB2 completely abolishes MET in auditory hair cells. However, MET is unaffected in *Cib2* knock-out vestibular hair cells (VHCs). In the present work, we show that CIB3 could compensate for the loss of CIB2 in VHCs, and *Cib2*/*Cib3* double knock-out completely abolishes MET in VHCs. Interestingly, CIB2 and CIB3 could also regulate VHC stereocilia maintenance in a nonredundant way. *Cib2* and *Cib3* transcripts are highly expressed in the striolar and extrastriolar regions, respectively. Stereocilia maintenance and balance function are differently affected in *Cib2* or *Cib3* knock-out mice. In conclusion, our data suggest that CIB2 and CIB3 are important for stereocilia maintenance and MET in mouse VHCs.

Received Sep. 22, 2022; revised Mar. 20, 2023; accepted Mar. 25, 2023.

Author contributions: Z.X. designed research; X.W., S.L., Q.C., C.Q., R.R., H.D., N.L., and K.Y. performed research; X.W., S.L., Q.C., C.Q., R.R., H.D., N.L., K.Y., Y.W., W.X., and Z.X. analyzed data; X.W., W.X., and Z.X. wrote the paper.

This work was supported by the National Key Research & Developmental Program of China Grant 2022YFE0131900 (to Z.X.), the China Ministry of Science and Technology Grant 2021ZD0203304 (to W.X.), National Natural Science Foundation of China Grants 82192861 and 82071051 (to Z.X.), the Shandong Provincial Natural Science Foundation Grant ZR2020ZD39 (to Z.X.), the Open Collaborative Research Program of Chinese Institute for Brain Research Grant 2020-NKX-XM-04 (to W.X.), and the China Postdoctoral Science Foundation Grant 2021M701920 (to S.L.). We thank Sen Wang, Xiaomin Zhao, and Haiyan Yu from the core facilities for life and environmental sciences, Shandong University for technical support in SEM and confocal microscopy.

*X.W. and S.L. contributed equally to this work.

The authors declare no competing financial interests.

Correspondence should be addressed to Wei Xiong at wei_xiong@cibr.ac.cn or Zhigang Xu at xuzg@sdu.edu.cn.

https://doi.org/10.1523/JNEUROSCI.1807-22.2023

Introduction

Hair cells are mechanosensory cells in the inner ear, responsible for hearing and balance perception. They are characterized by their apical cell protrusions referred to as the hair bundle, which consists of one tubulin-based kinocilium and dozens of actin-based stereocilia for each hair cell (Flock and Cheung, 1977). In mammalian auditory hair cells, stereocilia are organized into three rows of increasing height and transduce sound signals into electrical signals (Tilney et al., 1980). In mammalian vestibular hair cells (VHCs), stereocilia are organized into more rows of increasing height and transduce head movements into electrical signals (Krey and Barr-Gillespie, 2019). The development and maintenance of stereocilia are tightly regulated, and deficits in

these processes are usually associated with hearing loss and/or balance disorders (Barr-Gillespie, 2015; McGrath et al., 2017; Vélez-Ortega and Frolenkov, 2019).

In a single hair cell, the stereocilia are interconnected to each other through different types of extracellular links, among which tip-links connect the tips of shorter-row stereocilium to the lateral shaft of its neighboring taller stereocilium (Pickles et al., 1984; Goodyear et al., 2005). When the stereocilia are deflected toward the taller edge, the tension of tip-links increases, which in turn increases the open probability of the mechanoelectrical transduction (MET) channels, resulting in the influx of cations into hair cells (Hudspeth and Jacobs, 1979). Evidences suggest that transmembrane proteins cadherin 23 (CDH23) and protocadherin 15 (PCDH15) form the upper and lower parts of tip-links, respectively (Siemens et al., 2004; Kazmierczak et al., 2007). Moreover, the MET channels have been localized at the tips of shorter-row stereocilia and close to the lower end of tip links, and several MET complex components have been identified including TMC1/2, TMIE, and LHFPL5 (Beurg et al., 2009, 2015; Xiong et al., 2012; Kim and Fettiplace, 2013; Pan et al., 2013, 2018; Zhao et al., 2014; Corns et al., 2016; Ballesteros et al., 2018; Goldring et al., 2019; Cunningham et al., 2020; Jia et al., 2020).

Previously, we and others showed that calcium and integrin-binding protein 2 (CIB2) is a MET complex component (Giese et al., 2017; Michel et al., 2017; Wang et al., 2017). As a calcium-binding protein, CIB2 contains four EF-hand domains and is able to bind calcium through the last two domains, regions that are affected by several deafness-associated *CIB2* mutations (Blazejczyk et al., 2009; Riazuddin et al., 2012; Liang et al., 2021). CIB2 directly interacts with the putative pore-forming MET component TMC1/2 and is necessary for the correct localization of TMC1/2 in the stereocilia of auditory hair cells (Liang et al., 2021). In *Caenorhabditis elegans*, two copies of CIB2 homolog CALM-1, TMC-1 and TMIE were found to form a 2-fold symmetric complex (Jeong et al., 2022). Loss of CIB2 completely abolishes MET in auditory hair cells and leads to profound congenital hearing loss (Giese et al., 2017; Michel et al., 2017; Wang et al., 2017). However, CIB2 is not required for MET in VHCs as well as general balance function (Michel et al., 2017).

CIB2 belongs to a protein family with four members, CIB1 through CIB4 (Gentry et al., 2005), among which CIB2 and CIB3 are closest to each other (Wang et al., 2017). Differently from *Cib2* that is expressed both in the cochlea and vestibule, *Cib3* is mainly expressed in the vestibule (Giese et al., 2017; Wang et al., 2017). Furthermore, CIB3 can functionally substitute for CIB2 in injectoporated auditory hair cells (Liang et al., 2021). In the present work, we investigate the physiological role of CIB2 and CIB3 in VHCs using *Cib2*/*Cib3* single and double knock-out mice. The results show that loss of CIB2 or CIB3 differently affects VHC stereocilia maintenance, but does not affect MET in VHCs. However, simultaneous loss of CIB2 and CIB3 results in severe stereocilia maintenance deficits and complete loss of MET currents in VHCs, which account for profound balance deficits in *Cib2*/*Cib3* double knock-out mice.

Materials and Methods

Mice

The animal study was reviewed and approved by Animal Ethics Committee of Shandong University School of Life Sciences (Permission No. SYDWLL-2020-38). Mice of either sex were used in the present study. *Cib3* knock-out mice were generated using the clustered regularly interspaced short palindromic repeat (CRISPR)/CRISPR-associated protein 9 (Cas9) genome editing technique by Cyagen Biosciences Inc. Briefly, genomic DNA sequences 5′-CAGGTCGAGTCCCTCTTATG TGG-3′ and 5′-ATACGGCTGAGGTCATACACAGG-3′ were chosen as the guide RNA (gRNA) targets. *Cas9* mRNA and gRNAs were *in vitro* transcribed and injected into the cytoplasm of zygotes (C57BL/6N). After culturing *in vitro* for 24 h, the injected zygotes were transferred into the oviduct of a pseudopregnant ICR female mouse at 0.5 d postcoitus (dpc) to give rise to F0 mice, which were then crossed to wild-type (WT) C57BL/6N mice to give rise to heterozygous F1 mice. The following genotyping primers were used for examination of the knock-out allele: F1, 5′-AGGTTTTGTACTGAGGAACTTGTC-3′; R1, 5′-CTGCTCTTCACT TATCCATACATTC-3′; R2, 5′-AAAGTGACCTTCCAGTAGTCCTC-3′. A product of 403 base-pairs (bp) will be amplified from wild-type mice, and a product of 627 bp will be amplified from homozygote knock-out mice. Both products will be amplified from heterozygote knock-out mice. The deletion in *Cib3* genome was further confirmed by Sanger sequencing of the PCR product. $Cib2^{-/-}$ mice were maintained and genotyped as previously described (Wang et al., 2017). $Cib2^{-/-}$; $Cib3^{-/-}$ double knock-out mice were obtained by crossing $Cib3^{-/-}$ mice with $Cib2^{-/-}$ mice. Age-matched wild-type mice from an independent colony were also included as negative controls in some experiments of the present study.

RT-PCR

Total RNA of mouse inner ear was extracted using TRIzol reagent (Invitrogen) according to the manufacturer's protocol. Afterwards, 1 μg total RNA was used for RT using PrimeScript RT Reagent Kit with gDNA Eraser (Takara, RR047A). PCR was then performed using the RT product as template with the following primers: *Cib3*-F, 5′-TCTTCA CGAGGAAGGAGATC-3′; *Cib3*-R, 5′-TCAGATGCGGATGTGGAA GG-3′; β-*actin*-F, 5′-ACGGCCAGGTCATCACTATTG-3′; β-*actin*-R, 5′-AGGGGCCGGACTCATCGTA-3′.

Auditory brainstem response (ABR) measurements

Mice were anesthetized intraperitoneally with 8.4-mg pentobarbital/100 g body weight. Body temperature was maintained at 37°C by placing the mice on an isothermal pad during the experiment. A RZ6 workstation and BioSig software (Tucker-Davis Technologies) were used for stimulus generation, presentation, ABR acquisition, and data management. Acoustic stimuli in the form of clicks or tone bursts were generated using high-frequency transducers and delivered to the mouse ear through a loudspeaker (MF1, Tucker-Davis Technologies). At each sound level, 512 responses were sampled and averaged. ABR thresholds were obtained for each animal by reducing the stimulus intensity from 90 dB sound pressure level (SPL) in 10 dB SPL steps to identify the lowest intensity at which all ABR waves were detectable.

Vestibular function examination

Swimming test was performed in a rectangular tank (70 × 40 × 20 cm) filled with water at 30°C. Each mouse was tested three times of 30∼60 s with 5-min intervals. Scores were defined as follows: 0, normal swimming; 1, irregular swimming; 2, immobile floating; and 3, underwater tumbling. Rotarod test was performed as previously described with modifications (N. Li et al., 2021). Briefly, mice were placed in the rotarod apparatus (HB-600, Ruanlong) and the time before dropping from the rod was recorded. The experiment lasted seven consecutive days and testing data were recorded on the last 5 d. On each day, two training trials of 1 min at 10 revolutions per minute (rpm) were followed by three test trials that accelerate from 0 to 50 rpm over a 3-min period. The mice took a rest for 2 min between each trial. Balance beam test was performed as previously described (Luong et al., 2011). The balance beam of 80 cm long and 6 or 12 mm wide was placed 50 cm above ground with an escape box at one end. Mice were put at the other end of the beam and the time taken to reach the escape box was measured. Each mouse was tested three times and the average cross time was used as its score. Stereotyped circling movements (compulsive rotations of the body centered around the animal's hips) were recorded in the home cage.

Whole-mount in situ *hybridization*

Whole-mount *in situ* hybridization was performed as previously described with modifications (Zhang et al., 2020). Briefly, the coding

sequence (CDS) of mouse *Cib2*, *Cib3,* or *Tectb* gene was cloned into pZeroBack vector (Tiangen) then linearized to act as the template for probe transcription. Digoxigenin-labeled antisense probe was *in vitro* transcribed using DIG RNA labeling mix (Roche) according to the manufacturer's protocol. Mouse cochlear or vestibular sensory epithelia were dissected out and fixed with 4% paraformaldehyde (PFA), followed by incubation with 10 μg/ml proteinase K at 37°C for 10 min. The tissues were then incubated overnight at 60°C with digoxigenin-labeled probes, followed by incubation at 4°C overnight with anti-digoxigenin antibody (Roche). After signal development in NBT/BCIP solution (Roche), samples were mounted in 50% glycerol/PBS and imaged with an Olympus IX53 microscope.

Scanning electron microscopy (SEM)

Mouse temporal bone was dissected and fixed with 2.5% glutaraldehyde in 0.1 M phosphate buffer overnight at 4°C. Vestibular maculae were dissected out of the temporal bone, postfixed with 1% osmium tetroxide in 0.1 M phosphate buffer at 4°C for 2 h, followed by dehydration in ethanol and critically point drying using a Leica EM CPD300 (Leica). Samples were then mounted and sputter coated with platinum to a thickness of ~15 nm using a Cressington 108 sputter coater (Cressington). Images were taken using a Quanta250 field-emission scanning electron microscope (FEI). Striolar and extrastriolar cells were distinguished according to their localization and hair bundle morphology, as striola is localized in the central region of the maculae, and is characterized by the wider spacing and larger size of hair bundles; moreover, the identification of striolar hair bundles was assisted by their localization relative to the line of polarity reversal (LPR) of hair bundle orientation (Eatock and Songer, 2011; Ono et al., 2020a,b).

Injectoporation

Tissue culture and injectoporation was performed as previously described with modifications (Xiong et al., 2012, 2014). Briefly, utricular maculae were isolated from postnatal day (P)3 mice and cultured in DMEM/F12 with 1.5 μg/ml ampicillin. A glass pipette (2-μm tip diameter) was used to deliver plasmids (0.2 μg/μl in 1× HBSS) to hair cells in the maculae. A series of three pulses at 60 V lasting 15 ms at 1-s intervals were applied to tissues using an electroporator (ECM Gemini X2, BTX). The injectoporated tissues were cultured for 1 d before staining with TRITC-conjugated phalloidin (Sigma-Aldrich, P1951). After that, samples were mounted in 50% glycerol/PBS and imaged using a confocal microscope with a 1.4 NA/100× Kort M27 objective lens (LSM 700, Zeiss).

Electrophysiology

P6–P8 mice were euthanized and dissected to separate utricular maculae. Assisted by an upright microscope (BX51WI, Olympus) equipped with 60× water immersion objective (LUMPlanFL, Olympus), striolar and extrastriolar hair cells were distinguished by their location in the maculae, as well as hair bundle orientation and tissue thickness (Eatock and Songer, 2011; Ono et al., 2020a, b). In our analyses, Type I and Type II VHCs were not distinguished, largely because of lacking morphologic and electrophysiological characteristics at this age (Holt et al., 1997; Eatock and Songer, 2011). VHC electrophysiology was conducted as previously described with modifications (Wang et al., 2017). The recording solution contains 144 mM NaCl, 0.7 mM NaH_2PO_4, 5.8 mM KCl, 1.3 mM $CaCl_2$, 0.9 mM $MgCl_2$, 5.6 mM glucose, and 10 mM H-HEPES (pH 7.4). The pipette solution contains 140 mM KCl, 1 mM $MgCl_2$, 0.1 mM EGTA, 2 mM MgATP, 0.3 mM Na_2GTP, and 10 mM H-HEPES (pH 7.2). Patch pipettes were made from borosilicate glass capillaries (BF150-117-10, Sutter Instrument) with a pipette puller (P-2000, Sutter) and polished with a microforge (MF-830, Narishige) to resistances of 4–6 MΩ. Whole-cell recordings were conducted with an electrophysiology amplifier (EPC-10 USB, HEKA) controlled by the PatchMaster software with a holding potential of –70 mV. Recordings with series resistance <20 MΩ were saved for analysis. The average resting membrane potential is −66.8 mV for $Cib2^{-/-}$; $Cib3^{+/-}$ VHCs ($n = 8$), −67.7 mV for $Cib2^{+/-}$; $Cib3^{-/-}$ VHCs ($n = 7$), and −68.9 mV for $Cib2^{-/-}$; $Cib3^{-/-}$ VHCs ($n = 7$). The voltage-gated currents were recorded by delivering command voltages from −150 to +110 mV in 20-mV steps. For our whole cell measurement, the liquid junction was calculated as a value of +4 mV that has been subtracted in the data shown.

The MET currents were evoked using a fluid jet from a pipette (tip diameter of 5–10 μm) positioned facing the staircase side of the hair bundle at a distance of around 5 μm. The fluid flow was controlled by a 27-mm-diameter piezoelectric disk driven by a homemade 20× amplifier that precisely outputs analog driving voltage (Liu et al., 2019). The command signal was generated by EPC-10. To measure the maximal MET currents, a 140-V and 50-ms square-wave stimulation was given to the piezoelectric disk. This robust stimulation also causes irreversible damage on the target VHC's hair bundle. For the series stimulation, a family of 100-ms pulse signals from −10 to 35 V in 5-V steps were delivered to the piezoelectric disk. The interval between stimuli is 2 s to ensure that the hair bundle returns to initial state. With our fluid-jet apparatus, the step displacements driven by low voltages show delayed rise time, which becomes faster when the driver voltage increases. It is likely because that the puffing force is damped from the fluid-jet pipette on low driver voltage.

Statistical analysis

Data are shown as mean ± SEM. One-way ANOVA or two-way ANOVA with appropriate *post hoc* tests was used for statistical analysis as indicated in the figure legends, and $p < 0.05$ was considered statistically significant.

Results

Knock-out of *Cib2* gene affects stereocilia maintenance in striolar VHCs and leads to mild, late-onset balance deficits in mouse

We first examined the expression of *Cib2* transcripts in the sensory epithelia of cochlea, saccule, and utricle by performing *in situ* hybridization. Probes against *Tectb* were used to label the striolar region of saccule and utricle (Rau et al., 1999). The results showed that *Cib2* transcripts are specifically expressed in the hair cell region of the cochlea at P4 (Fig. 1*A*). In the saccule and utricle at P4, *Cib2* transcripts were strongly detected in the striolar region (Fig. 1*B*). No signal was detected in the *Cib2* knock-out organs, confirming the specificity of the probes (Fig. 1*A*,*B*). Because our antibody against CIB2 does not work well in whole-mount immunostaining of vestibular organs, we employed injectoporation assay to examine the localization of CIB2 in the VHCs. The results revealed that when overexpressed in the VHCs, GFP-tagged CIB2 is localized at the tips of stereocilia (Fig. 1*C*).

Balance functions of the knock-out mice were then evaluated by performing two commonly used standard tests, namely the rotarod test and the swimming test. Neither test revealed any balance deficits in *Cib2* knock-out mice up to age of six months (Fig. 1*D*,*E*). However, by age of nine months, mild balance deficit in *Cib2* knock-out mice could be detected by the swimming test (Fig. 1*E*). The balance beam test has been used to evaluate subtle balance deficits that usually cannot be detected by standard tests (Luong et al., 2011; Ono et al., 2020b). We then performed balance beam test, which also revealed mild deficits in *Cib2* knock-out mice at age of nine months (Fig. 1*F*,*G*). Therefore, our present results suggest that *Cib2* knock-out mice show mild, late-onset balance deficits.

SEM was then performed to examine the stereocilia morphology of VHCs in *Cib2* knock-out mice. Extrastriolar VHC stereocilia in $Cib2^{-/-}$ saccules are morphologically comparable to that in $Cib2^{+/-}$ and wild-type saccules when examined at P30 (Fig. 2*A*). However, striolar VHC stereocilia in $Cib2^{-/-}$ saccules are less organized at this age (Fig. 2*A*). It has been reported that there is considerable variety in the morphology of VHC hair bundles,

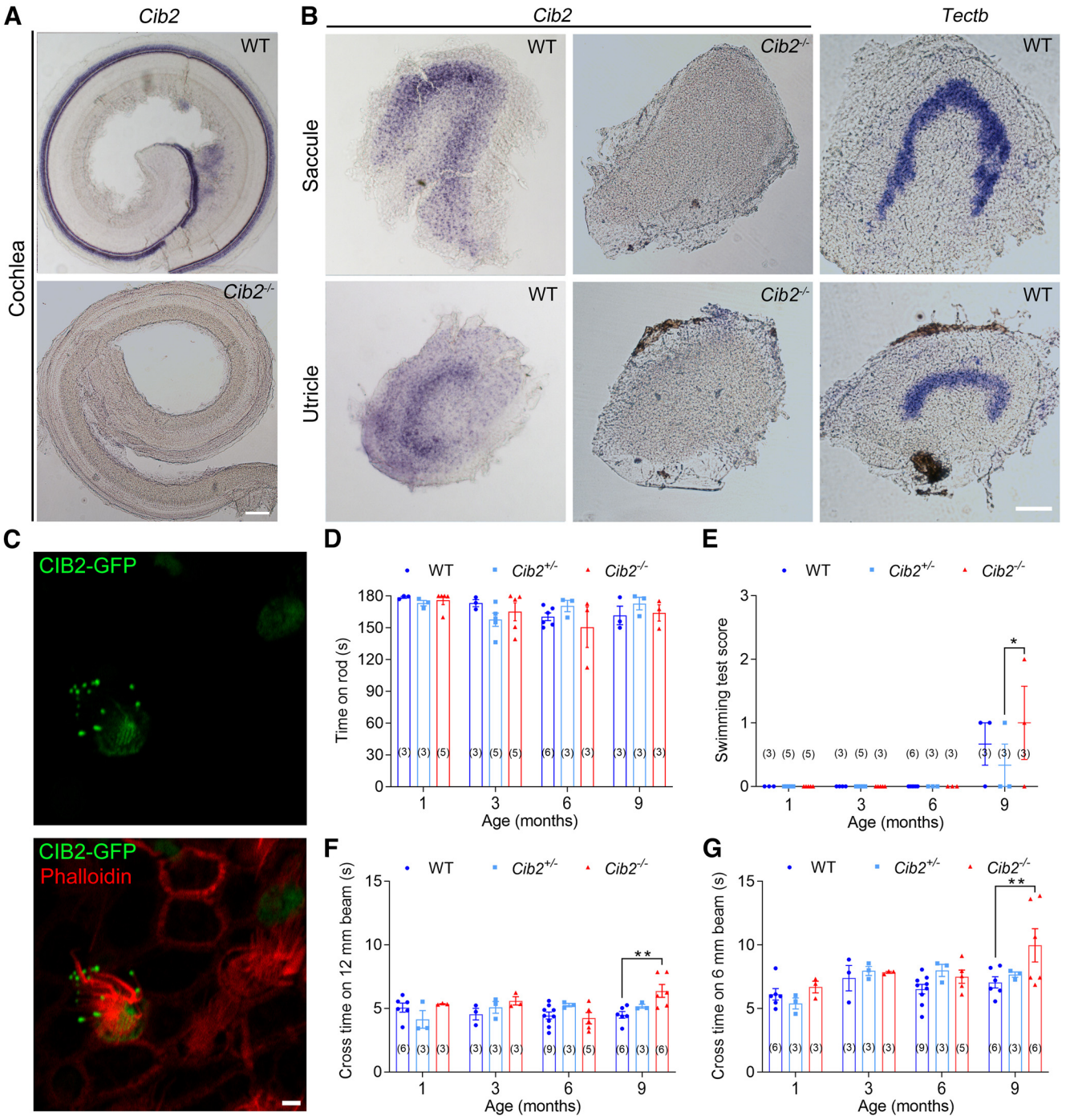

Figure 1. Knock-out of *Cib2* leads to mild, late-onset balance deficits. ***A***, ***B***, Expression of *Cib2* transcripts in the cochlea (***A***) and vestibule (saccule and utricle; ***B***) of wild-type or $Cib2^{-/-}$ mice at P4 were examined by performing *in situ* hybridization. Probes against *Tectb* were used to label the striolar region of saccule and utricle. ***C***, Utricular explants from wild-type mice at P3 were injectoporated with expression vectors to express GFP-tagged CIB2 in hair cells and imaged using a confocal microscope. GFP fluorescence (green) indicates the subcellular localization of CIB2. Stereociliary F-actin core is visualized by TRITC-conjugated phalloidin (red). ***D–G***, Balance function of $Cib2^{-/-}$ or control mice was evaluated by performing rotarod test (***D***), swimming test (***E***), 12-mm-wide balance beam test (***F***), and 6-mm-wide balance beam test (***G***) at different ages as indicated. The numbers of mice used in each group are indicated in brackets. Scale bars, 100 μm (***A***, ***B***), 2 μm (***C***). *$p < 0.05$, **$p < 0.01$; no significant difference is detected in all the unlabeled comparisons (two-way ANOVA with Tukey's test).

such as tall v.s. short stereocilia as well as tight v.s. loose configuration (Bagger-Sjöbäck and Takumida, 1988; A. Li et al., 2008). The disorganized stereocilia bundles in $Cib2^{-/-}$ mice further increase the complexity of bundle morphology. Therefore, we did not distinguish different types of stereocilia in the present work; instead, we picked multiple hair bundles randomly for each position from each genotype and quantified the numbers of stereocilia per VHC. At P30, ~40 stereocilia are present in each wild-type VHCs in the striolar and extrastrolar regions of saccules and utricles (Fig. 2*A*,*C*). However, stereocilia numbers are significantly decreased in the striolar VHCs of both saccules and utricles in P30 $Cib2^{-/-}$ mice compared with that in wild-type mice (WT saccule = 37.0 ± 1.0 vs $Cib2^{-/-}$ saccule = 27.8 ± 1.4, $p < 0.0001$; WT utricle = 42.4 ± 1.0 vs $Cib2^{-/-}$ utricle = 20.7 ± 1.4, $p < 0.0001$, according to two-way ANOVA with Tukey's test). Interestingly, striolar VHC

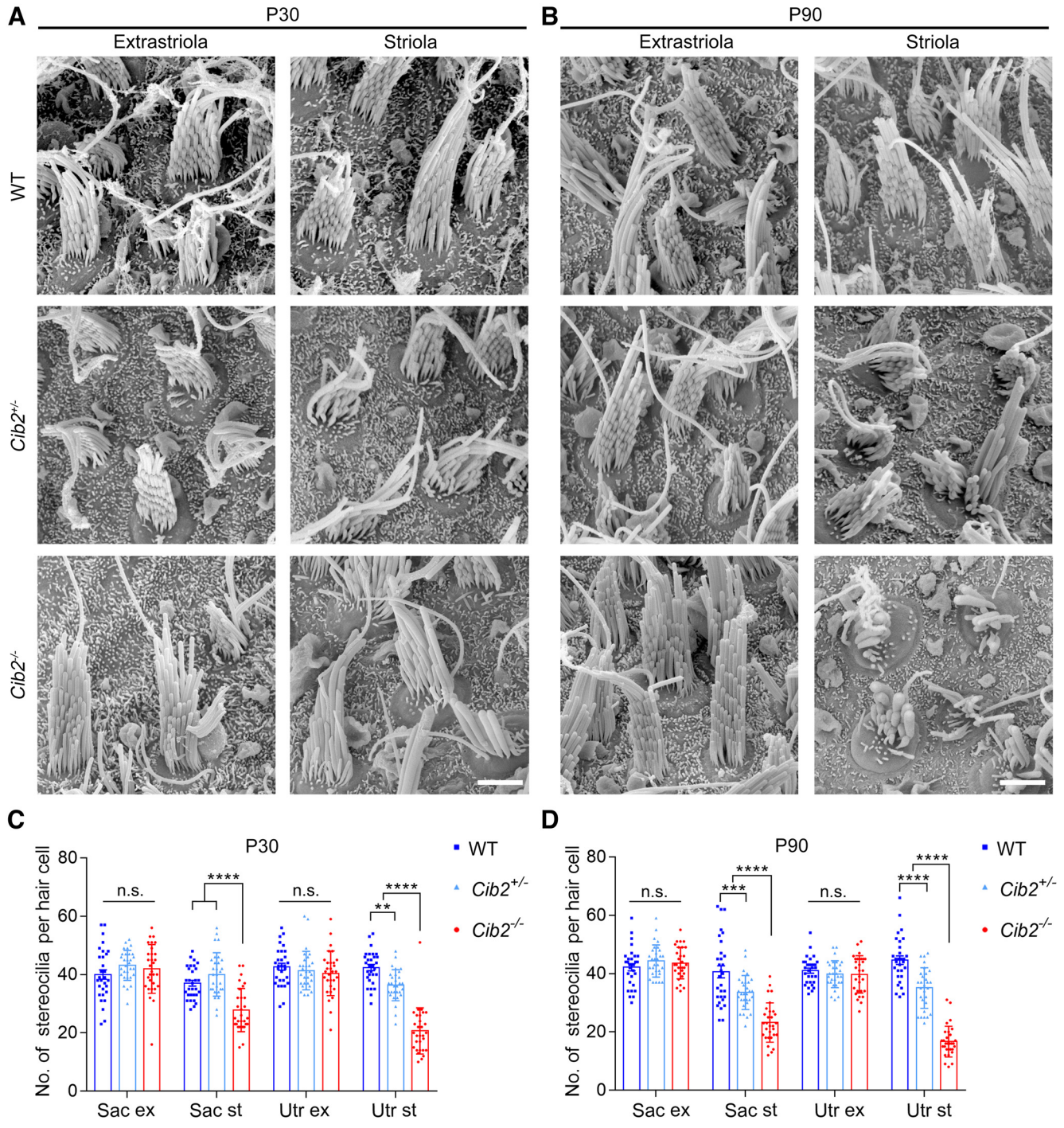

Figure 2. Knock-out of *Cib2* affects stereocilia maintenance in striolar VHCs. ***A***, ***B***, SEM was employed to examine the hair bundles of saccular VHCs from extrastriolar or striolar regions of wild-type, $Cib2^{+/-}$, and $Cib2^{-/-}$ mice at P30 (***A***) and P90 (***B***). ***C***, ***D***, Analysis of stereocilia numbers of VHCs from extrastriolar or striolar regions of wild-type, $Cib2^{+/-}$, and $Cib2^{-/-}$ saccule and utricle at P30 (***C***) and P90 (***D***) according to the SEM results. For each group, 30 cells from three mice were analyzed. Scale bars, 2 μm. n.s., not significant; $^{**}p < 0.01$, $^{***}p < 0.001$, $^{****}p < 0.0001$ (two-way ANOVA with Tukey's test).

stereocilia in $Cib2^{+/-}$ utricles also show decreased numbers compared with that in wild-type utricles, albeit to a lesser extent (WT utricle = 42.4 ± 1.0 vs $Cib2^{+/-}$ utricle = 36.4 ± 1.0, $p < 0.01$ according to two-way ANOVA with Tukey's test; Fig. 2*C*). The stereocilia number is further decreased in $Cib2^{-/-}$ and $Cib2^{+/-}$ striolar VHCs when examined at P90, while no significant difference is detected in extrastriolar VHCs up to this age (Fig. 2*B*,*D*). Taken together, our present data suggest that loss of CIB2 affects stereocilia maintenance in striolar VHCs.

Knock-out of *Cib3* gene affects stereocilia maintenance in VHCs and leads to progressive balance deficits in mouse

The expression pattern of *Cib3* transcripts in the mouse inner ear was examined by performing *in situ* hybridization. The results revealed that *Cib3* transcripts are not expressed in the cochlea, while are enriched in the extrastriolar region of saccule and utricle (Fig. 3*A*,*B*). Without specific anti-CIB3 antibodies to hand, we performed injectoporation experiments to examine the subcellular localization of CIB3 in the VHCs. The results showed

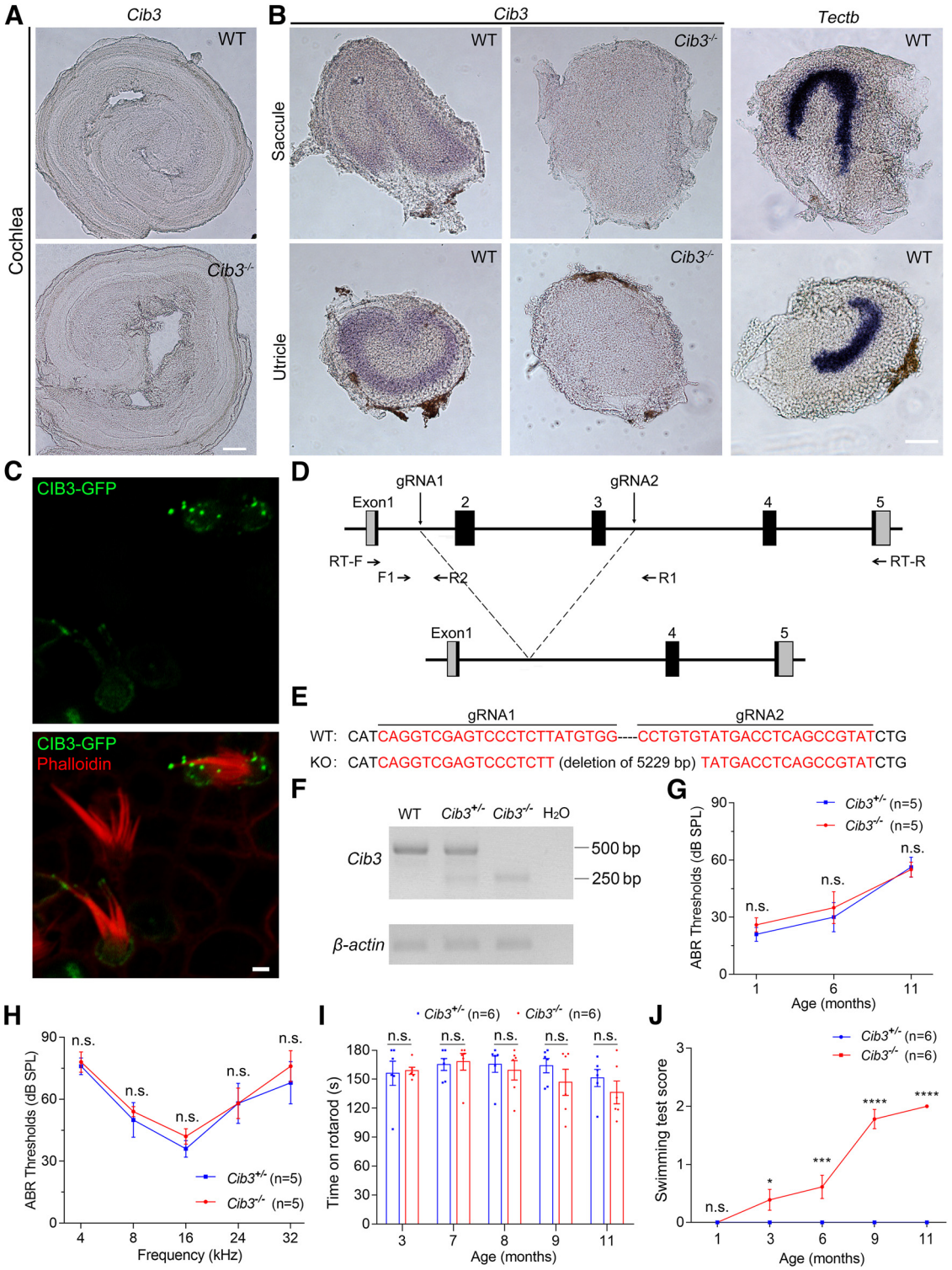

Figure 3. Knock-out of *Cib3* leads to progressive balance deficits. ***A***, ***B***, Expression of *Cib3* transcripts in the cochlea (***A***) and vestibule (saccule and utricle; ***B***) of wild-type or $Cib3^{-/-}$ mice at P1 were examined by performing *in situ* hybridization. Probes against *Tectb* were used to label the striolar region of saccule and utricle. ***C***, Utricular explants from wild-type mice at P3 were injectoporated with expression vectors to express GFP-tagged CIB3 in hair cells and imaged using a confocal microscope. GFP fluorescence (green) indicates the subcellular localization of CIB3. Stereociliary F-actin core is visualized by TRITC-conjugated phalloidin (red). ***D***, Schematic drawing of the strategy for construction of *Cib3* knock-out mice. The positions of gRNAs and PCR primers are indicated by arrows. ***E***, Sanger sequencing results reveal a deletion of 5229 bp in the genome of *Cib3* knock-out mice. Targeting sites of gRNAs are indicated in red. ***F***, Expression of *Cib3* mRNA in the inner ear of P30 mice was examined by performing RT-PCR using RT-F and RT-R as primers. *β-actin* was included as the internal control. ***G***, ABR thresholds to click stimuli of $Cib3^{+/-}$ and $Cib3^{-/-}$ mice at different ages as indicated. ***H***, ABR thresholds to pure tone stimuli of nine-month-old $Cib3^{+/-}$ and $Cib3^{-/-}$ mice. ***I***, ***J***, Balance function of $Cib3^{+/-}$ and $Cib3^{-/-}$ mice at different ages as indicated was evaluated by performing rotarod test (***I***) and swimming test (***J***). The numbers of mice used in each group are indicated in brackets. Scale bars, 100 μm (***A***, ***B***), 2 μm (***C***). n.s., not significant; *$p < 0.05$, ***$p < 0.001$, ****$p < 0.0001$ (two-way ANOVA with Sidak's test).

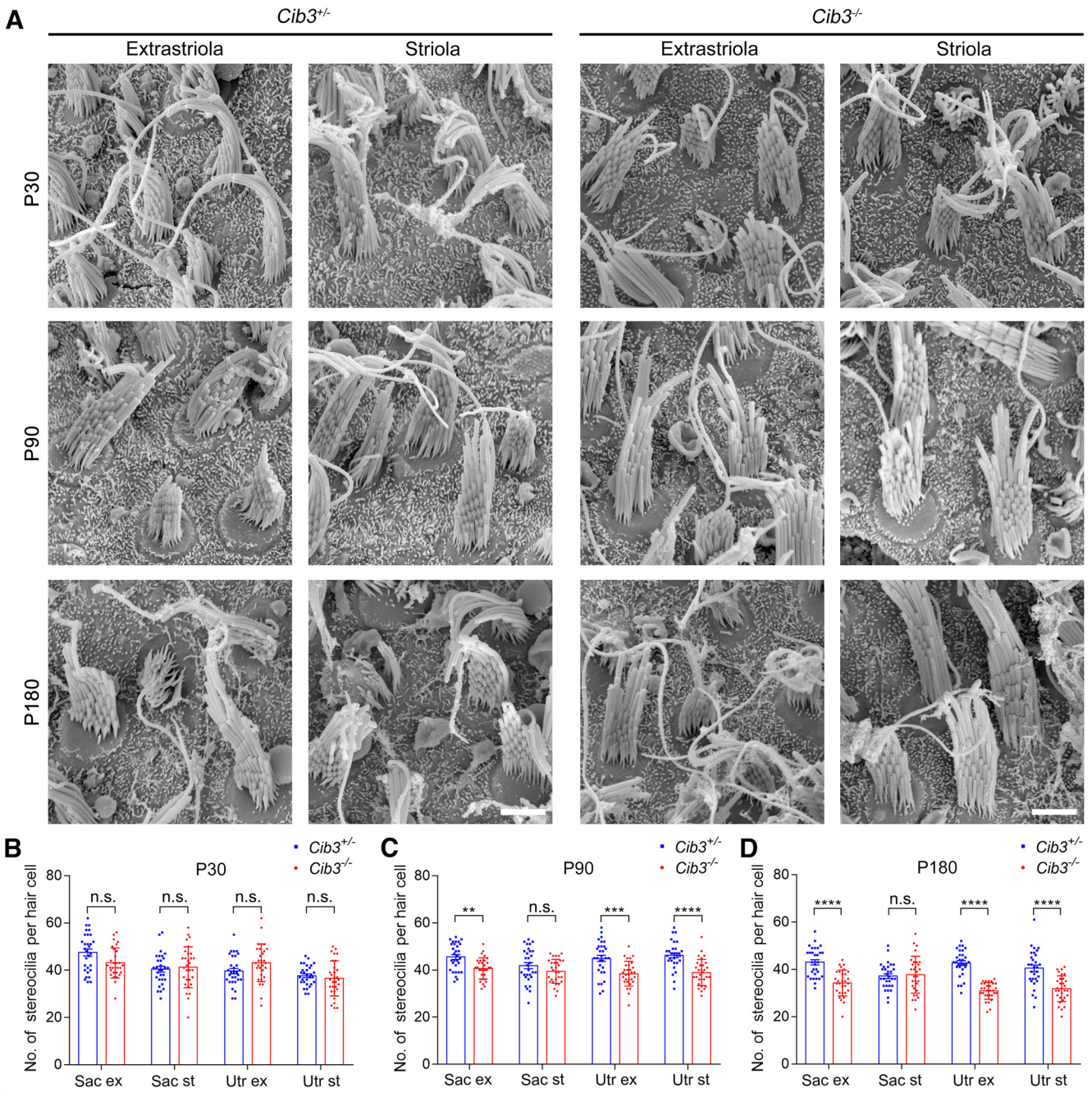

Figure 4. Knock-out of *Cib3* affects stereocilia maintenance in VHCs. ***A***, SEM was employed to examine the hair bundles of saccular VHCs of $Cib3^{+/-}$ and $Cib3^{-/-}$ mice at different ages as indicated. ***B–D***, Analysis of stereocilia numbers of VHCs from striolar or extrastriolar regions of $Cib3^{+/-}$ and $Cib3^{-/-}$ saccule and utricle at P30 (***B***), P90 (***C***), and P180 (***D***) according to the SEM results. For each group, 30 cells from three mice were analyzed. Scale bars, 2 μm. n.s., not significant; $^{**}p < 0.01$, $^{***}p < 0.001$, $^{****}p < 0.0001$ (two-way ANOVA with Sidak's test).

that injectoporated CIB3-GFP is localized at the tips of the stereocilia in VHCs (Fig. 3*C*), in a pattern similar to CIB2-GFP (Fig. 1*C*).

To investigate the potential role of CIB3 in balance perception, we established *Cib3* knock-out mice using the CRISPR/Cas9 genome editing technique. Mouse *Cib3* gene contains five exons, with the translational start codon localized in exon 1 and the translational stop codon in exon 5 (Fig. 3*D*). Two gRNAs were used to delete exons 2 and 3 that cover 54.17% of the coding sequence of *Cib3* gene (Fig. 3*D*). The deletion of exons 2 and 3 was confirmed by genotyping PCR and Sanger sequencing (Fig. 3*E*). RT-PCR was performed to examine the expression of *Cib3* transcripts in the *Cib3* knock-out mice. The two primers used to amplify the *Cib3* transcripts are localized at exon 1 and 5, respectively, which will give rise to a PCR product of 503 bp in wild-type mice or a potential PCR product of 243 bp in *Cib3* knock-out mice (Fig. 3*D*). Two PCR products with the expected size were amplified from the wild-type mice and knock-out mice, respectively; however, the knock-out band is very weak, suggesting that *Cib3* transcripts in the knock-out mice undergo nonsense-mediated mRNA decay (NMD; Fig. 3*F*). *In situ* hybridization results also support loss of *Cib3* transcripts in the knock-out mice (Fig. 3*B*).

The auditory function of *Cib3* knock-out mice was evaluated by performing ABR measurements, which reveal normal hearing

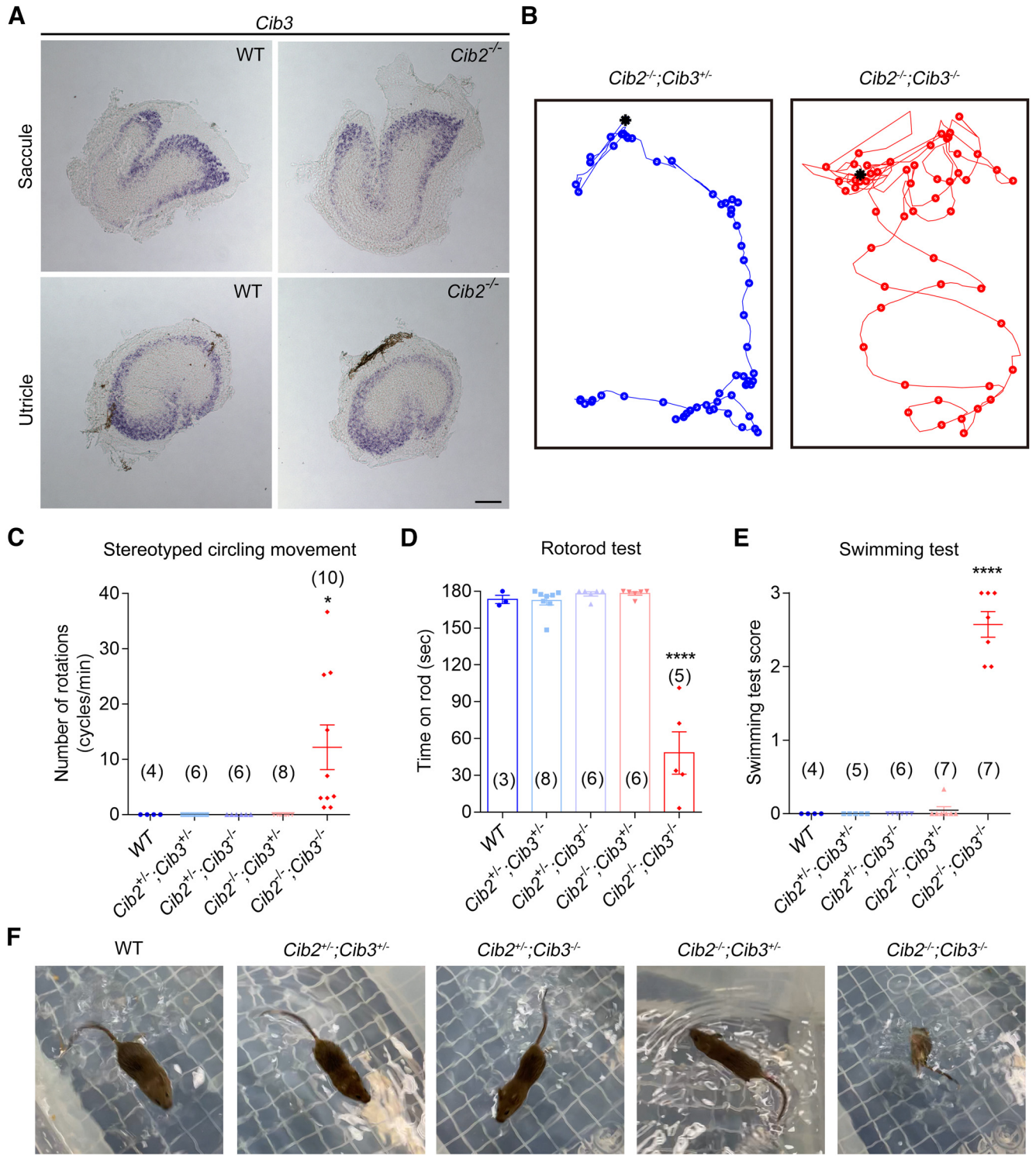

Figure 5. *Cib2*/*Cib3* double knock-out significantly affects balance function in mouse. ***A***, Expression of *Cib3* transcripts in the saccule and utricle of wild-type and $Cib2^{-/-}$ mice at P1 was examined by performing *in situ* hybridization. Scale bar, 100 μm. ***B***, Representative examples of locomotion of $Cib2^{-/-}$; $Cib3^{+/-}$ and $Cib2^{-/-}$; $Cib3^{-/-}$ mice at P30 in a 10-s period. Asterisk indicates the starting position, and dots indicate the locations of the mouse every 0.166 s. ***C–E***, Balance function of mice of different genotypes at P30 was evaluated by performing stereotyped circling movement test (***C***), rotarod test (***D***), and swimming test (***E***). ***F***, Images of swimming posture of mice of different genotypes at P30. The numbers of mice used in each group were indicated in brackets. *$p < 0.05$, ****$p < 0.0001$ (one-way ANOVA with Dunnett's test).

threshold of $Cib3^{-/-}$ mice up to age of 11 months (Fig. 3*G*,*H*). Rotarod test suggests that $Cib3^{-/-}$ mice have mild albeit statistically insignificant balance deficit started at age of eight months (Fig. 3*I*). Swimming test further confirms that balance deficit could be detected in $Cib3^{-/-}$ mice as early as three months and is further exaggerated when the mice age (Fig. 3*J*). Taken together, our present data suggest that *Cib3* knock-out causes progressive balance deficits in mouse.

The hair bundle of *Cib3* knock-out VHCs was then examined by performing SEM. At age of P30, stereocilia number of $Cib3^{-/-}$ VHCs is comparable to that of $Cib3^{+/-}$ VHCs (Fig. 4*A*,*B*). However, stereocilia number of P90 $Cib3^{-/-}$ mice is slightly but

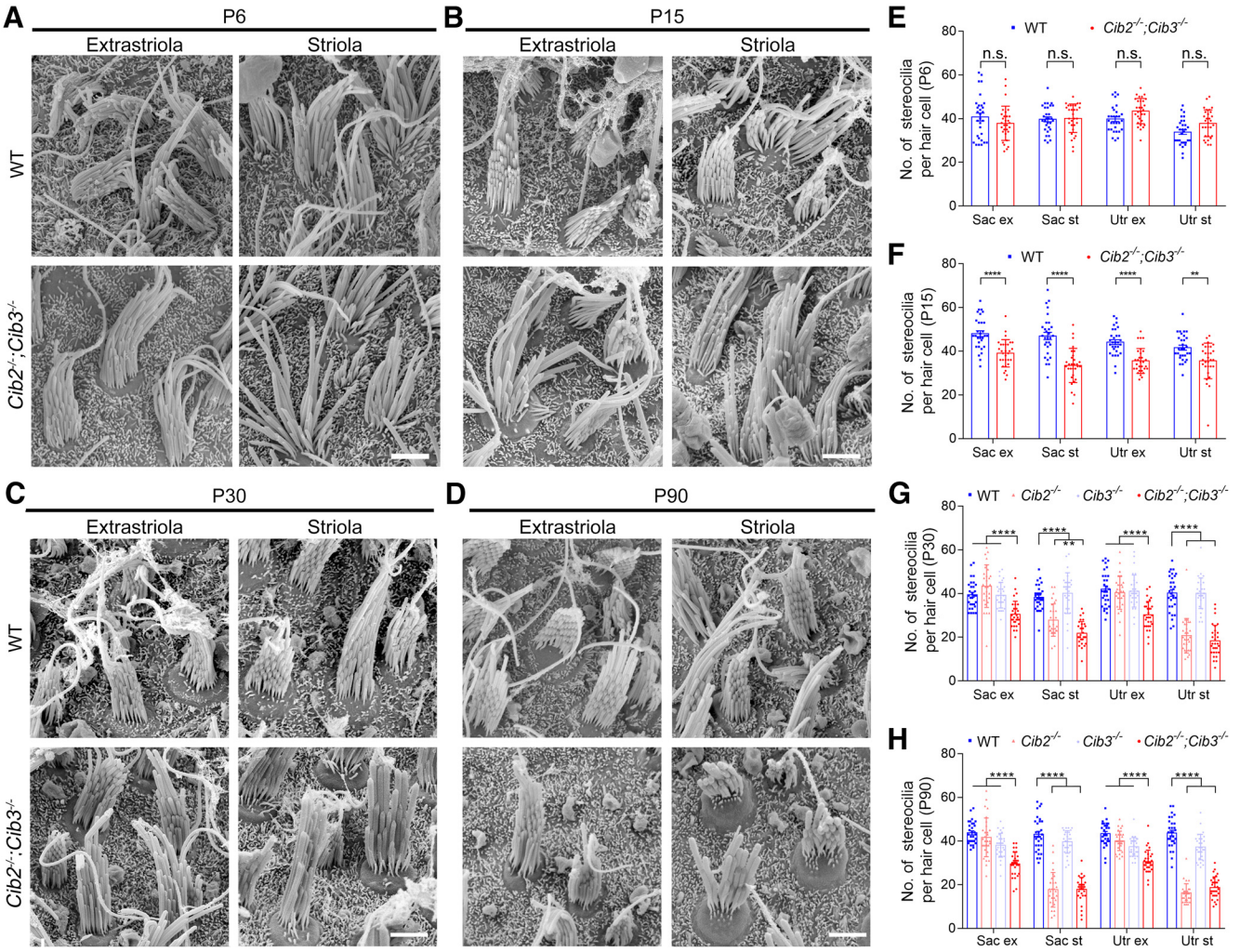

Figure 6. *Cib2*/*Cib3* double knock-out significantly affects stereocilia maintenance in VHCs. ***A–D***, SEM was employed to examine the hair bundles of saccular VHCs from extrastriolar or striolar regions of wild-type and $Cib2^{-/-}$; $Cib3^{-/-}$ mice at P6 (***A***), P15 (***B***), P30 (***C***), and P90 (***D***). ***E–H***, Analysis of stereocilia numbers of VHCs from extrastriolar or striolar regions of mice of different genotypes at P6 (***E***), P15 (***F***), P30 (***G***), and P90 (***H***) according to the SEM results. For each group, 30 cells from three mice were analyzed. Scale bars, 2 μm. n.s., not significant; $^{**}p < 0.01$, $^{****}p < 0.0001$ (two-way ANOVA with Sidak's test in ***E***, ***F***; two-way ANOVA with Tukey's test in ***G***, ***H***).

statistically significantly decreased compared with that of $Cib3^{+/-}$ mice in the utricle as well as in the extrastriolar region of saccule ($p < 0.01$ according to two-way ANOVA with Sidak's test; Fig. 4*A*,*C*), suggesting that *Cib3* knock-out affects stereocilia maintenance in VHCs. The stereocilia loss is further exaggerated in $Cib3^{-/-}$ mice by P180 (Fig. 4*A*,*D*). Therefore, our present data suggest that loss of CIB3 modestly affects stereocilia maintenance in VHCs at elder ages.

$Cib2^{-/-}$; $Cib3^{-/-}$ double knock-out significantly affects stereocilia maintenance and balance functions

So far, our data suggest that $Cib3^{-/-}$ mice show progressive balance deficits, while mild balance deficits could only be detected in $Cib2^{-/-}$ mice after age of six months. Considering that both *Cib2* and *Cib3* transcripts are expressed in the vestibular maculae albeit enriched in different subregions, we wanted to know whether *Cib3* expression is upregulated in $Cib2^{-/-}$ vestibules by performing *in situ* hybridization. The results show that *Cib3* expression is largely unaffected in the saccules and utricles of $Cib2^{-/-}$ mice (Fig. 5*A*). Next, by crossing $Cib3^{-/-}$ mice with $Cib2^{-/-}$ mice, we obtained $Cib2^{-/-}$; $Cib3^{-/-}$ double knock-out mice. At age of P30, $Cib2^{-/-}$; $Cib3^{-/-}$ mice manifest typical stereotyped circling movement, while $Cib2^{-/-}$ and $Cib3^{-/-}$ single knock-out mice do not (Fig. 5*B*,*C*). Severe balance deficits in $Cib2^{-/-}$; $Cib3^{-/-}$ mice were further confirmed by rotarod test and swimming test (Fig. 5*D–F*).

SEM results show that stereocilia number is unaffected in VHCs of $Cib2^{-/-}$; $Cib3^{-/-}$ mice at P6 (Fig. 6*A*,*E*). However, significant stereocilia loss could be observed in both the striolar and extrastriolar regions of saccules and utricles in $Cib2^{-/-}$; $Cib3^{-/-}$ mice at P15 (Fig. 6*B*,*F*). Stereocilia loss is further exaggerated when examined in $Cib2^{-/-}$; $Cib3^{-/-}$ VHCs at P30 and P90 (Fig. 6*C*,*D*,*G*,*H*). Notably, *Cib2* knock-out and *Cib3* knock-out differently affect stereocilia maintenance in striolar and extrastriolar VHCs. In striolar VHCs, stereocilia loss is mainly caused by *Cib2* knock-out, as comparable stereocilia loss were observed in $Cib2^{-/-}$ and $Cib2^{-/-}$; $Cib3^{-/-}$ striolar VHCs (Fig. 6*G*,*H*). In contrast, significant stereocilia loss in extrastriolar VHCs is only observed in $Cib2^{-/-}$; $Cib3^{-/-}$ mice by P90 (Fig. 6*G*,*H*). Taken together, our present data suggest that $Cib2^{-/-}$; $Cib3^{-/-}$ double knock-out significantly affects VHC stereocilia maintenance as well as balance functions.

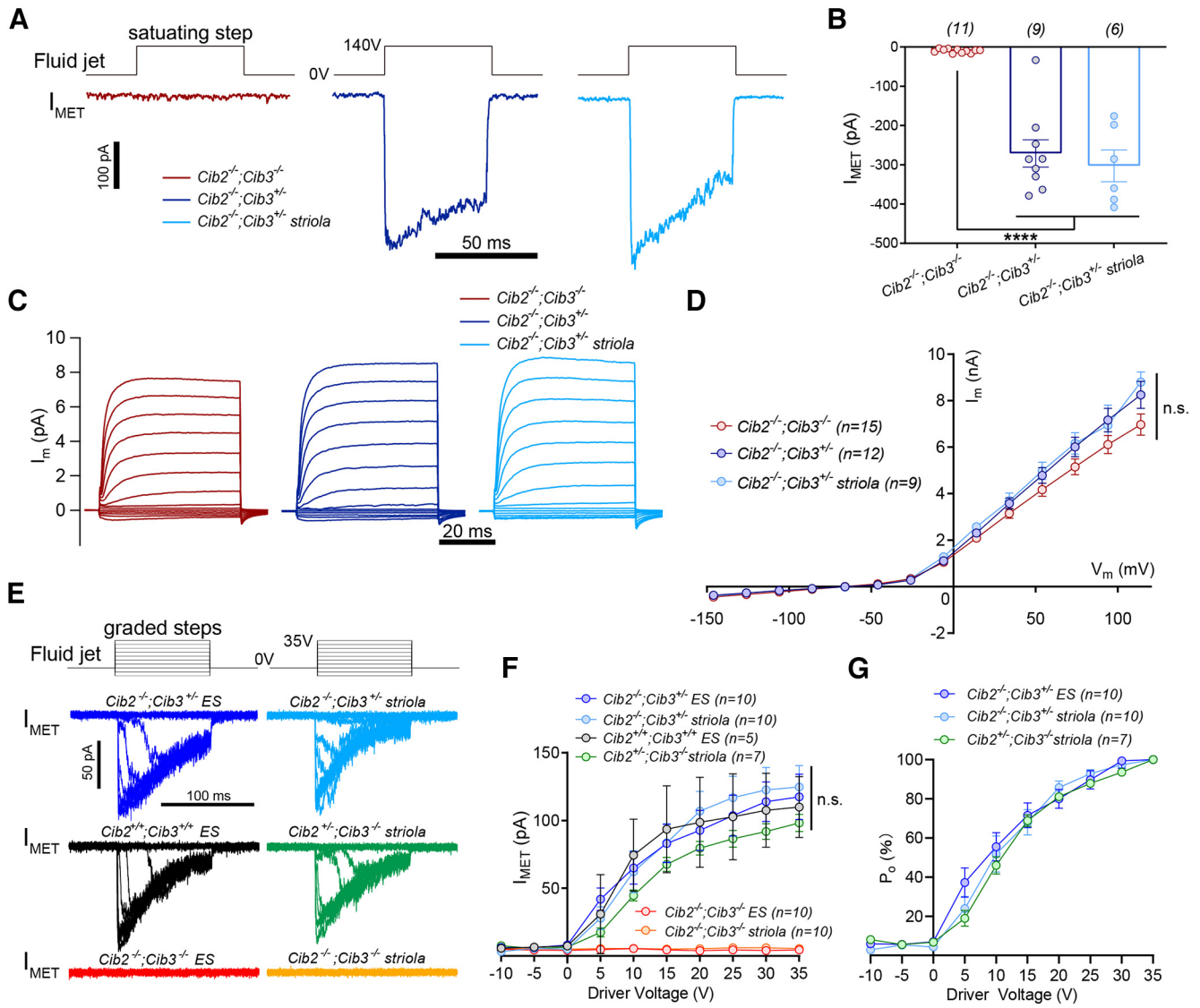

Figure 7. MET currents are abolished in *Cib2*/*Cib3* double knock-out VHCs. ***A***, Maximal MET currents were recorded in P6-P8 VHCs from $Cib2^{-/-}$; $Cib3^{-/-}$ and $Cib2^{-/-}$; $Cib3^{+/-}$ mice. An overstimulated one-time step fluid-jet was used to evoke the maximal MET currents from VHCs. ***B***, Average peak current was quantified from the results similar to ***A***. ***C***, Voltage-gated currents were recorded in P6-P8 VHCs from $Cib2^{-/-}$; $Cib3^{-/-}$ and $Cib2^{-/-}$; $Cib3^{+/-}$ mice. The membrane potential was changed from −150 to +110 mV in 20-mV steps. ***D***, Current–voltage (I–V) curves were drawn from the results similar to ***C***. In ***A–D***, striolar VHCs (cyan) from $Cib2^{-/-}$; $Cib3^{+/-}$ mice were distinguished and evaluated as an individual group. ***E***, Representative MET currents recorded from P6-P8 $Cib2^{+/+}$; $Cib3^{+/+}$, $Cib2^{-/-}$; $Cib3^{+/-}$, $Cib2^{+/-}$; $Cib3^{-/-}$, and $Cib2^{-/-}$; $Cib3^{-/-}$ VHCs in striolar and extrastriolar (ES) regions. A series of mild steps at graded intensities were delivered by fluid jet to evoke the incremental MET currents from VHCs. ***F***, Quantification of peak amplitude of evoked MET currents from similar recordings shown in ***E***. ***G***, Normalized peak amplitude of evoked MET currents from similar recordings shown in ***E***. The numbers of cells are indicated in the brackets, which were collected from no less than three mice for each condition. n.s., not significant; **** $p < 0.0001$ (one-way ANOVA with Brown–Forsythe test).

MET currents are completely abolished in $Cib2^{-/-}$; $Cib3^{-/-}$ VHCs

To examine how MET is affected in $Cib2^{-/-}$; $Cib3^{-/-}$ VHCs, we recorded the MET currents in VHCs whose hair bundles were deflected with a fluid-jet system. We first randomly picked VHCs at P6-P8 with no discrimination in striolar or extrastriolar regions and measured their maximal MET currents by delivering a one-time overstimulated step displacement. The results show that the MET currents are completely abolished in $Cib2^{-/-}$; $Cib3^{-/-}$ VHCs (Fig. 7*A*,*B*), reminiscent of our previous recordings in $Cib2^{-/-}$ OHCs (Wang et al., 2017). However, in $Cib2^{-/-}$; $Cib3^{+/-}$ mice, an average MET current of around 270 pA was recorded (Fig. 7*A*,*B*), comparable to the result from wild-type VHCs (Caprara and Peng, 2022). Considering that *Cib2* transcripts are enriched in striolar VHCs, we then recorded the MET currents specifically in $Cib2^{-/-}$; $Cib3^{+/-}$ striolar VHCs. The results show that MET currents clearly remain normal in $Cib2^{-/-}$; $Cib3^{+/-}$ striolar VHCs (Fig. 7*A*,*B*). Furthermore, we measured the voltage-gated currents, which are unaffected in $Cib2^{-/-}$; $Cib3^{-/-}$ VHCs (Fig. 7*C*,*D*).

To further examine how CIB2 and CIB3 influence the MET kinetics, we used a series of mild steps with graded intensities to stimulate the VHCs. The MET currents were recorded in striolar and extrastriolar VHCs from $Cib2^{+/+}$; $Cib3^{+/+}$, $Cib2^{-/-}$; $Cib3^{+/-}$, $Cib2^{+/-}$; $Cib3^{-/-}$, and $Cib2^{-/-}$; $Cib3^{-/-}$ mice (Fig. 7*E*). In $Cib2^{-/-}$; $Cib3^{-/-}$ mice, neither striolar VHCs nor extrastriolar VHCs show detectable MET currents (Fig. 7*E*,*F*). In $Cib2^{+/+}$; $Cib3^{+/+}$, $Cib2^{-/-}$; $Cib3^{+/-}$, and $Cib2^{+/-}$; $Cib3^{-/-}$ mice, both striolar and extrastriolar VHCs have plateau MET currents with amplitude from

100 pA to 120 pA (Fig. 7*E*,*F*), similarly to previous observation in wild-type VHCs (Holt et al., 1997). The average amplitude increment and open probability of the MET currents are indistinguishable among *Cib2*$^{+/+}$; *Cib3*$^{+/+}$, *Cib2*$^{-/-}$; *Cib3*$^{+/-}$, and *Cib2*$^{+/-}$; *Cib3*$^{-/-}$ VHCs (Fig. 7*F*,*G*). Therefore, our present data suggest that CIB2 and CIB3 are functionally redundant in regulating MET in VHCs.

Discussion

CIB2 was recently shown to play important roles in MET, as loss of CIB2 completely abolishes MET currents in auditory hair cells and causes profound congenital hearing loss (Giese et al., 2017; Michel et al., 2017; Wang et al., 2017). Further investigations suggested that CIB2 binds putative pore-forming MET components TMC1 and TMC2, and regulates their localization to the stereocilia (Liang et al., 2021). However, MET currents in VHCs and general balance function were found to be unaffected in *Cib2* knock-out mice (Michel et al., 2017). CIB3, a homolog of CIB2, can functionally substitute for CIB2 in injectoporated auditory hair cells (Liang et al., 2021). *Cib2* is expressed in both the cochlea and vestibule, while *Cib3* is mainly expressed in the vestibule (Giese et al., 2017; Wang et al., 2017), consistent with the hypothesis that CIB2 and CIB3 might act redundantly to regulate MET in VHCs. Here, in the present work, we show that *Cib2*/*Cib3* double knock-out completely abolishes MET currents in VHCs, supporting the conclusion that CIB2 and CIB3 together are indispensable for MET in VHCs.

CIB2 and CIB3 belong to a protein family with four members (CIB1–CIB4) that share multiple calcium-binding EF-hand domains (Gentry et al., 2005). Besides *Cib2* and *Cib3*, *Cib1* is expressed in both the cochlea and vestibule, while *Cib4* is not detected in the inner ear (Wang et al., 2017). Previously we have shown that, despite its expression in the inner ear, CIB1 is not necessary for auditory function (Wang et al., 2017). Moreover, MET currents are completely abolished in the auditory hair cells of *Cib2* knock-out mice (Wang et al., 2017) as well as in the VHCs of *Cib2*/*Cib3* double knock-out mice (the present work), further supporting the conclusion that CIB1 cannot compensate for the loss of CIB2 and/or CIB3. In line with this, co-immunoprecipitation results confirm that CIB2 and CIB3 but not CIB1 interact with the putative pore-forming MET component TMC1 (Liang et al., 2021).

Interestingly, our *in situ* hybridization results show that *Cib2* and *Cib3* transcripts have complementary expression patterns in the vestibular maculae. *Cib2* transcripts are strongly expressed in the striolar region and weakly expressed in the extrastriolar region. In contrast, *Cib3* transcripts are enriched in the extrastriolar region. Striolar VHCs differ from extrastriolar VHCs in several aspects, such as hair bundle morphology and electrophysiological properties, among others (Lim, 1984; Goldberg et al., 1990; A. Li et al., 2008; Lysakowski et al., 2011). Striolar VHCs and their associated afferents are more sensitive to higher-frequency head motion (Baird et al., 1988; Goldberg et al., 1990; Eatock, 2018). Consistent with the striolar expression of *Cib2*, our present work uncovered that CIB2 is required for stereocilia maintenance in striolar VHCs. A similar scenario has been reported in *Cytochrome P450 26b1* (*Cyp26b1*) conditional knock-out mice (Ono et al., 2020b). CYP26B1 mediates degradation of retinoic acid (RA), which has been shown to play important roles in striola formation (Ono et al., 2020a,b). Whether *Cib2* expression in the striola is regulated through RA signaling pathway is an interesting question and awaits further investigation. *Cyp26b1* knock-out leads to deficits in challenging balance functions that was revealed by balance beam tests (Ono et al., 2020b). It remains elusive why *Cib2*$^{-/-}$ mice do not show obvious balance deficits before age of six months although loss of CIB2 significantly affects stereocilia maintenance in striolar VHCs during early adulthood.

Considering the complementary expression pattern of *Cib2* and *Cib3* transcripts in the vestibular maculae, it is quite surprising that CIB2 and CIB3 act redundantly in regulating MET in VHCs. One possibility is that low expression level of CIB2 or CIB3 is enough for MET function. Therefore, in the striolar VHCs, low expression of CIB3 is able to support MET function in *Cib2*$^{-/-}$ mice. Similarly, in the extrastriolar VHCs, low expression of CIB2 is able to support MET function in *Cib3*$^{-/-}$ mice. On the other hand, high expression level of CIB2 or CIB3 might be required for stereocilia maintenance in the striolar or extrastriolar VHCs, respectively. In line with this hypothesis, stereocilia maintenance deficits are detected in the striolar VHCs of *Cib2*$^{-/-}$ mice as well as in the extrastriolar VHCs of *Cib3*$^{-/-}$ mice. CIB2 expression level is particularly critical for striolar VHC stereocilia maintenance, as significant stereocilia deficits could be observed even in *Cib2*$^{+/-}$ striolar VHCs.

At present, the mechanism underlying how CIB2 and CIB3 regulate stereocilia morphology remains elusive. Evidences suggest that MET affects stereocilia development and/or maintenance (Vélez-Ortega et al., 2017; Krey et al., 2020). When MET is inhibited pharmacologically by MET blockers or genetically by knock-out of genes essential for MET, stereocilia morphology in auditory hair cells is significantly altered (Vélez-Ortega et al., 2017; Krey et al., 2020). However, the stereocilia phenotype in *Cib2* or *Cib3* knock-out VHCs cannot be explained by MET deficits, given that VHCs deficient for *Cib2* or *Cib3* have normal MET currents when examined at P6-P8. Previously, we proposed that CIB2 could regulate stereocilia maintenance in auditory hair cells through interacting with BAIAP2L2 (Yan et al., 2022a). BAIAP2L2 is a recently-identified row 2 complex component that localizes at the tips of shorter-row, mechanotransducing stereocilia, and loss of BAIAP2L2 results in degeneration of shorter-row stereocilia as well as hearing loss (Carlton et al., 2021; Yan et al., 2022a). Furthermore, stereociliary tip localization of BAIAP2L2 is disrupted in *Cib2* knock-out mice (Yan et al., 2022a). These data are consistent with the hypothesis that CIB2 regulates stereocilia maintenance directly through binding to row 2 complex component BAIAP2L2 at least in auditory hair cells.

However, the stereocilia phenotype in *Cib2* knock-out striolar VHCs cannot be simply explained by a BAIAP2L2-dependent mechanism, since we have shown that BAIAP2L2 is dispensable for stereocilia development/maintenance in VHCs (Yan et al., 2022b). Loss of row 2 complex components other than BAIAP2L2, such as EPS8L2 or MYO15A-L, also has no effect on VHC stereocilia morphology or vestibular function (Furness et al., 2013; Fang et al., 2015). A possible explanation is that other protein(s) could substitute for BAIAP2L2 in VHCs, and loss of CIB2 affects all of them therefore leads to VHC stereocilia deficits. Further investigations are required to identify the mechanism underlying how CIB2/CIB3 regulates stereocilia maintenance in VHCs.

References

Bagger-Sjöbäck D, Takumida M (1988) Geometrical array of the vestibular sensory hair bundle. Acta Otolaryngol 106:393–403.

Baird RA, Desmadryl G, Fernández C, Goldberg JM (1988) The vestibular nerve of the chinchilla. II. Relation between afferent response properties and peripheral innervation patterns in the semicircular canals. J Neurophysiol 60:182–203.

Ballesteros A, Fenollar-Ferrer C, Swartz KJ (2018) Structural relationship between the putative hair cell mechanotransduction channel TMC1 and TMEM16 proteins. Elife 7:e38433.

Barr-Gillespie PG (2015) Assembly of hair bundles, an amazing problem for cell biology. Mol Biol Cell 26:2727–2732.

Beurg M, Fettiplace R, Nam JH, Ricci AJ (2009) Localization of inner hair cell mechanotransducer channels using high-speed calcium imaging. Nat Neurosci 12:553–558.

Beurg M, Xiong W, Zhao B, Müller U, Fettiplace R (2015) Subunit determination of the conductance of hair-cell mechanotransducer channels. Proc Natl Acad Sci U S A 112:1589–1594.

Blazejczyk M, Sobczak A, Debowska K, Wisniewska MB, Kirilenko A, Pikula S, Jaworski J, Kuznicki J, Wojda U (2009) Biochemical characterization and expression analysis of a novel EF-hand Ca^{2+} binding protein calmyrin2 (Cib2) in brain indicates its function in NMDA receptor mediated Ca^{2+} signaling. Arch Biochem Biophys 487:66–78.

Caprara GA, Peng AW (2022) Mechanotransduction in mammalian sensory hair cells. Mol Cell Neurosci 120:103706.

Carlton AJ, Halford J, Underhill A, Jeng JY, Avenarius MR, Gilbert ML, Ceriani F, Ebisine K, Brown SDM, Bowl MR, Barr-Gillespie PG, Marcotti W (2021) Loss of Baiap2l2 destabilizes the transducing stereocilia of cochlear hair cells and leads to deafness. J Physiol 599:1173–1198.

Corns LF, Johnson SL, Kros CJ, Marcotti W (2016) Tmc1 point mutation affects Ca^{2+} sensitivity and block by Dihydrostreptomycin of the mechanoelectrical transducer current of mouse outer hair cells. J Neurosci 36:336–349.

Cunningham CL, Qiu XF, Wu ZZ, Zhao B, Peng GH, Kim YH, Lauer A, Müller U (2020) TMIE defines pore and gating properties of the mechanotransduction channel of mammalian cochlear hair cells. Neuron 107:126–143.e8.

Eatock RA (2018) Specializations for fast signaling in the amniote vestibular inner ear. Integr Comp Biol 58:341–350.

Eatock RA, Songer JE (2011) Vestibular hair cells and afferents: two channels for head motion signals. Annu Rev Neurosci 34:501–534.

Fang Q, Indzhykulian AA, Mustapha M, Riordan GP, Dolan DF, Friedman TB, Belyantseva IA, Frolenkov GI, Camper SA, Bird JE (2015) The 133-kDa N-terminal domain enables myosin 15 to maintain mechanotransducing stereocilia and is essential for hearing. Elife 4:e08627.

Flock A, Cheung HC (1977) Actin-filaments in sensory hairs of inner-ear receptor cells. J Cell Biol 75:339–343.

Furness DN, Johnson SL, Manor U, Rüttiger L, Tocchetti A, Offenhauser N, Olt J, Goodyear RJ, Vijayakumar S, Dai Y, Hackney CM, Franz C, Di Fiore PP, Masetto S, Jones SM, Knipper M, Holley MC, Richardson GP, Kachar B, Marcotti W (2013) Progressive hearing loss and gradual deterioration of sensory hair bundles in the ears of mice lacking the actin-binding protein Eps8L2. Proc Natl Acad Sci U S A 110:13898–13903.

Gentry HR, Singer AU, Betts L, Yang C, Ferrara JD, Sondek J, Parise LV (2005) Structural and biochemical characterization of CIB1 delineates a new family of EF-hand-containing proteins. J Biol Chem 280:8407–8415.

Giese APJ, Tang YQ, Sinha GP, Bowl MR, Goldring AC, Parker A, Freeman MJ, Brown SDM, Riazuddin S, Fettiplace R, Schafer WR, Frolenkov GI, Ahmed ZM (2017) CIB2 interacts with TMC1 and TMC2 and is essential for mechanotransduction in auditory hair cells. Nat Commun 8:43.

Goldberg JM, Desmadryl G, Baird RA, Fernández C (1990) The vestibular nerve of the chinchilla. V. Relation between afferent discharge properties and peripheral innervation patterns in the utricular macula. J Neurophysiol 63:791–804.

Goldring AC, Beurg M, Fettiplace R (2019) The contribution of TMC1 to adaptation of mechanoelectrical transduction channels in cochlear outer hair cells. J Physiol 597:5949–5961.

Goodyear RJ, Marcotti W, Kros CJ, Richardson GP (2005) Development and properties of stereociliary link types in hair cells of the mouse cochlea. J Comp Neurol 485:75–85.

Holt JR, Corey DP, Eatock RA (1997) Mechanoelectrical transduction and adaptation in hair cells of the mouse utricle, a low-frequency vestibular organ. J Neurosci 17:8739–8748.

Hudspeth AJ, Jacobs R (1979) Stereocilia mediate transduction in vertebrate hair-cells. Proc Natl Acad Sci U S A 76:1506–1509.

Jeong H, Clark S, Goehring A, Dehghani-Ghahnaviyeh S, Rasouli A, Tajkhorshid E, Gouaux E (2022) Structures of the TMC-1 complex illuminate mechanosensory transduction. Nature 610:796–803.

Jia YY, Zhao YM, Kusakizako T, Wang Y, Pan CF, Zhang YW, Nureki O, Hattori M, Yan ZQ (2020) TMC1 and TMC2 proteins are pore-forming subunits of mechanosensitive ion channels. Neuron 105:310–321.e3.

Kazmierczak P, Sakaguchi H, Tokita J, Wilson-Kubalek EM, Milligan RA, Müller U, Kachar B (2007) Cadherin 23 and protocadherin 15 interact to form tip-link filaments in sensory hair cells. Nature 449:87–91.

Kim KX, Fettiplace R (2013) Developmental changes in the cochlear hair cell mechanotransducer channel and their regulation by transmembrane channel-like proteins. J Gen Physiol 141:141–148.

Krey JF, Barr-Gillespie PG (2019) Molecular composition of vestibular hair bundles. Cold Spring Harb Perspect Med 9:a033209.

Krey JF, Chatterjee P, Dumont RA, O'Sullivan M, Choi D, Bird JE, Barr-Gillespie PG (2020) Mechanotransduction-dependent control of stereocilia dimensions and row identity in inner hair cells. Curr Biol 30:442–454.e7.

Li A, Xue J, Peterson EH (2008) Architecture of the mouse utricle: macular organization and hair bundle heights. J Neurophysiol 99:718–733.

Li N, Xi Y, Du H, Zhou H, Xu Z (2021) Annexin A4 is dispensable for hair cell development and function. Front Cell Dev Biol 9:680155.

Liang X, Qiu X, Dionne G, Cunningham CL, Pucak ML, Peng G, Kim YH, Lauer A, Shapiro L, Müller U (2021) CIB2 and CIB3 are auxiliary subunits of the mechanotransduction channel of hair cells. Neuron 109:2131–2149.e15.

Lim DJ (1984) Otoconia in health and disease. A review. Ann Otol Rhinol Laryngol 93:17–24.

Liu S, Wang S, Zou L, Li J, Song C, Chen J, Hu Q, Liu L, Huang P, Xiong W (2019) TMC1 is an essential component of a leak channel that modulates tonotopy and excitability of auditory hair cells in mice. Elife 8:e47441.

Luong TN, Carlisle HJ, Southwell A, Patterson PH (2011) Assessment of motor balance and coordination in mice using the balance beam. J Vis Exp 49:2376.

Lysakowski A, Gaboyard-Niay S, Calin-Jageman I, Chatlani S, Price SD, Eatock RA (2011) Molecular microdomains in a sensory terminal, the vestibular calyx ending. J Neurosci 31:10101–10114.

McGrath J, Roy P, Perrin BJ (2017) Stereocilia morphogenesis and maintenance through regulation of actin stability. Semin Cell Dev Biol 65:88–95.

Michel V, et al. (2017) CIB2, defective in isolated deafness, is key for auditory hair cell mechanotransduction and survival. EMBO Mol Med 9:1711–1731.

Ono K, Sandell LL, Trainor PA, Wu DK (2020a) Retinoic acid synthesis and autoregulation mediate zonal patterning of vestibular organs and inner ear morphogenesis. Development 147:dev192070.

Ono K, Keller J, López Ramírez O, Garrido AG, Zobeiri OA, Chang HHV, Vijayakumar S, Ayiotis A, Duester G, Della Santina CC, Jones SM, Cullen KE, Eatock RA, Wu DK (2020b) Retinoic acid degradation shapes zonal development of vestibular organs and sensitivity to transient linear accelerations. Nat Commun 11:63.

Pan B, Géléoc GS, Asai Y, Horwitz GC, Kurima K, Ishikawa K, Kawashima Y, Griffith AJ, Holt JR (2013) TMC1 and TMC2 are components of the mechanotransduction channel in hair cells of the mammalian inner ear. Neuron 79:504–515.

Pan B, Akyuz N, Liu XP, Asai Y, Nist-Lund C, Kurima K, Derfler BH, György B, Limapichat W, Walujkar S, Wimalasena LN, Sotomayor M, Corey DP, Holt JR (2018) TMC1 forms the pore of mechanosensory transduction channels in vertebrate inner ear hair cells. Neuron 99:736–753.e6.

Pickles JO, Comis SD, Osborne MP (1984) Cross-links between stereocilia in the guinea-pig organ of Corti, and their possible relation to sensory transduction. Hear Res 15:103–112.

Rau A, Legan PK, Richardson GP (1999) Tectorin mRNA expression is spatially and temporally restricted during mouse inner ear development. J Comp Neurol 405:271–280.

Riazuddin S, et al. (2012) Alterations of the CIB2 calcium- and integrin-binding protein cause Usher syndrome type 1J and nonsyndromic deafness DFNB48. Nat Genet 44:1265–1271.

Siemens J, Lillo C, Dumont RA, Reynolds A, Williams DS, Gillespie PG, Müller U (2004) Cadherin 23 is a component of the tip link in hair-cell stereocilia. Nature 428:950–955.

Tilney LG, Derosier DJ, Mulroy MJ (1980) The organization of actin-filaments in the stereocilia of cochlear hair-cells. J Cell Biol 86:244–259.

Vélez-Ortega AC, Frolenkov GI (2019) Building and repairing the stereocilia cytoskeleton in mammalian auditory hair cells. Hear Res 376:47–57.

Vélez-Ortega AC, Freeman MJ, Indzhykulian AA, Grossheim JM, Frolenkov GI (2017) Mechanotransduction current is essential for stability of the transducing stereocilia in mammalian auditory hair cells. Elife 6:e24661.

Wang Y, Li J, Yao X, Li W, Du H, Tang M, Xiong W, Chai R, Xu Z (2017) Loss of CIB2 causes profound hearing loss and abolishes mechanoelectrical transduction in mice. Front Mol Neurosci 10:401.

Xiong W, Grillet N, Elledge HM, Wagner TFJ, Zhao B, Johnson KR, Kazmierczak P, Müller U (2012) TMHS is an integral component of the mechanotransduction machinery of cochlear hair cells. Cell 151:1283–1295.

Xiong W, Wagner T, Yan L, Grillet N, Müller U (2014) Using injectoporation to deliver genes to mechanosensory hair cells. Nat Protoc 9:2438–2449.

Yan K, Zong W, Du H, Zhai X, Ren R, Liu S, Xiong W, Wang Y, Xu Z (2022a) BAIAP2L2 is required for the maintenance of mechanotransducing stereocilia of cochlear hair cells. J Cell Physiol 237:774–788.

Yan K, Qu C, Wang Y, Zong W, Xu Z (2022b) BAIAP2L2 inactivation does not affect stereocilia development or maintenance in vestibular hair cells. Front Mol Neurosci 15:829204.

Zhang Y, Wang YF, Yao XB, Wang CQ, Chen FY, Liu D, Shao M, Xu ZG (2020) Rbm24a is necessary for hair cell development through regulating mRNA stability in zebrafish. Front Cell Dev Biol 8:604026.

Zhao B, Wu Z, Grillet N, Yan L, Xiong W, Harkins-Perry S, Müller U (2014) TMIE is an essential component of the mechanotransduction machinery of cochlear hair cells. Neuron 84:954–967.